Influence of Zr element on the atomic structure of Al-Cu alloy liquid

Saichao Cao, Mingxu Xia, Noel Jakse, Long Zeng, Pengfei Yu, Yimeng Zhao, Wenquan Lu, Jianguo Li

Influence of Zr element on the atomic structure of Al-Cu alloy liquid

Saichao Cao[1], Mingxu Xia[1], Noel Jakse[2], Long Zeng[1], Pengfei Yu[1], Yimeng Zhao[1], Wenquan Lu[1], and Jianguo Li[1]

[1] School of Materials Science and Engineering, Shanghai Jiao Tong University, Shanghai 200240, China

[2] University Grenoble Alpes, CNRS, SIMaP, Grenoble INP, F-38000 Grenoble, France

ABSTRACT

The correlation between structure and glass-forming ability in multicomponent alloys is a long-standing puzzle due to the complexity of compositions. In this work, $Al_{77.8}Cu_{22.2}$ and $Al_{70}Cu_{20}Zr_{10}$ amorphous alloy liquids were investigated by combining high-energy X-ray diffraction at a synchrotron facility, *ab-initio* molecular dynamics and reverse Monte Carlo simulations. The short- and medium-range order structures of two alloy liquids were analyzed and compared. The results suggest that the glass-forming ability of Al-Cu-Zr alloy liquid is not related to the content of icosahedral short-range order, but to the diversity of cluster types and the uniformity of cluster content distribution, and the structural heterogeneity and correlation of clusters with high five-fold symmetry. These findings reveal the role of Zr element in enhancing the glass-forming ability of Al-Cu alloy liquid, and deepen the understanding of Al-based metallic glasses formation.

· Corresponding author.

Email address: mingxu.xia@sjtu.edu.cn (Mingxu Xia), noel.jakse@grenoble-inp.fr (Noel Jakse)

Due to the special structure and properties [1,2], metallic glass has attracted a lot of attention since its discovery. Understanding the atomic structure and formation mechanism of metallic glass is the basis for the design and development of new materials, which has been also a challenging hot topic in condensed matter physics and material science from a fundamental point of view. In the past few decades, significant progress was made in this field. Some structure models such as the cluster dense packing model [3] and quasi-equivalent cluster model [4] were successively built to understand atomic packing. Several empirical rules for the design to improve the glass-forming ability (GFA) have been also proposed [5,6], such as the negative heat of formation, and a large difference in the atomic size of the constituent. However, the structural origin of GFA is still not fully understood, especially for the multicomponent alloy systems.

Many multicomponent alloys with good GFA have been found and studied [7]. Among these alloy systems, Al-early transition metal (EM)-late transition metal (LM) and Al-transition metal (TM)-rare-earth metal (RE) alloys are a special class of members due to their ability to form metallic glasses in both Al-rich and Al-poor regions, such as Al-Cu-Zr [7,8], Al-Ni-La [9,10] alloys. A large number of studies [11-13] have been carried out for metallic glasses in Al-poor regions. For example, Cheng *et al.* [12] investigated the structure of $Cu_{46}Zr_{47}Al_7$ and $Cu_{46}Zr_{54}$ metallic glasses, and found that a small addition of Al element can dramatically increase the population of full icosahedra and their spatial connectivity, and Cu- (and Al-) centered icosahedral clusters are identified as the basic local structural motifs in $Cu_{46}Zr_{47}Al_7$. These results provide a good description of the atomic structure and explain the enhanced GFA with a small addition of Al element. However, there is still a lack of corresponding studies on the role of small amounts of elements in enhancing the GFA for the Al-rich region at present. Although previous study [14] has indicated that the interaction among EM, Al, and Fe elements plays an important role in $Al_{70}Fe_{20}EM_{10}$ (EM=Ti, Zr, Hf, V and Cr) metallic glasses, it lacks the rationale at the atomic scale.

To address this issue, *ab initio* molecular dynamics (AIMD) simulation is usually the most powerful and reliable approach as it can provide high accuracy of atomic interactions. However, simulations with only 200~300 atoms with a few solute atoms can be currently performed, the statistical fluctuation could thus be significant [12]. On the other hand, reverse Monte Carlo (RMC) simulation allow to obtain larger atomic configurations and improve the reliability of the data [15,16], but chosen constraints, and non-unicity makes it questionable and should be assessed more deeply.

In this paper, $Al_{77.8}Cu_{22.2}$ (atomic ratio of 7:2) and $Al_{70}Cu_{20}Zr_{10}$ alloy liquids above liquidus temperature, T_l, are investigated through high-energy X-ray diffraction (HE-XRD) at a synchrotron facility for this purpose. In order to have a deeper view on the experimental features, a combination of AIMD and RMC simulations are carried out to ensure the consistency of the investigated atomic configurations. The short- and medium-range orders of two alloy liquids were analyzed and compared by common neighbor analysis (CNA), five-fold symmetry and a cluster correlation method. Our results show that the GFA of Al-Cu-Zr amorphous alloy liquid is not related to the content of icosahedral short-range order (ISRO), but to the diversity of cluster types and the uniformity of cluster content distribution, and the structural heterogeneity and correlation of clusters with high five-fold symmetry.

$Al_{77.8}Cu_{22}$ and $Al_{70}Cu_{20}Zr_{10}$ alloy compositions (~10 g) were prepared by induction melting of pure (99.999% purity) elements Al, Cu and Zr in a high purity Ar (99.999%) atmosphere. Samples of 2 mm cubes were cut from the solidified alloy ingots and used for HE-XRD analysis on BL13W1 at Shanghai synchrotron radiation facility (SSRF). Melting and cooling of the specimens were performed on a corundum substrate using an FSTi100SWB SYNRAD laser heating (100 Watts) device (heating rate: 30 K/s) and cooling (cooling rate: 10 K/s), in a vacuum of chamber (10^{-3} Pa) with refilled high purity Ar atmosphere. The temperature of the sample was recorded using a pyrometer with an accuracy of ± 5 K. High-energy (69.525 keV, 0.178454 Å) X-ray diffraction studies were made in a transmission geometry to high scattering

wave vector, q (16 $Å^{-1}$), using a Perkin Elmer Si 1621 detector. Diffractograms were measured for the alloy compositions at five temperatures: 225 K, 175 K, 125 K, 75 K and 25 K above liquidus temperature, T_l, and obtained by taking 30-second exposures per temperature step. According to the phase diagram, T_l of the two alloys is approximately 844 K and 1609 K, respectively. The raw diffraction data were integrated using the *Fit2D* program [17] to obtain diffraction intensity as a function of q. The structure factors, $S(q)$s, and pair correlation functions, $g(r)$s, are extracted after corrections to those data were made for background scattering from the air, absorption effects, polarization, multiple scattering, and Compton scattering contributions using the *PDFgetX2* [18] analysis package.

AIMD simulations of $Al_{77.8}Cu_{22.2}$ and $Al_{70}Cu_{20}Zr_{10}$ alloy liquids were carried out with the Vienna *Ab initio* Simulation Package (VASP) code [19]. All the simulations were performed in the local density approximation [20] and using projected augmented plane-waves with a plane-wave cutoff of 350 eV. Newton's equations of motion were integrated using Verlet's algorithm in the velocity form with a time step of 1.5 fs within the NVT ensemble, by means of a Nose thermostat to control temperature. A number of 256 atoms with the experimental compositions are arranged in a cubic simulation box with standard periodic boundary conditions. Only the Γ point is used to sample the Brillouin zone. The liquid samples were first prepared at a temperature well above the highest one studied, then followed by a cooling to the successive lower desired temperatures for the given alloy. At each temperature, the cell size was adjusted to make the average internal pressure close to zero within ±1 GPa, and more than 20000 timesteps were carried out to reach thermal equilibrium. I.S.A.A.C.S. program [21] is used for the calculation of structure factors and pair-correlation functions.

Atomic structures were obtained by RMC [22] fits to the measured X-ray static structure factors, $S(q)$s, while constraining the simulation with partial $g(r)$s obtained from AIMD simulations. The latter provide partial $g(r)$s, out to 12 Å. The description and details of the constrained RMC technique can be found in the RMC_POT user

guide. For this study, random starting configurations of 10000 atoms with the corresponding stoichiometric composition of the alloys were used. Periodic boundary conditions were applied in all three directions and the cubic box length was selected to fit the atomic number density obtained from the AIMD simulations. The minimum cutoff distances of atom pairs were also set according to the partial $g(r)$s obtained from AIMD simulation. The RMC simulation fits were performed three times from different initial atomic configurations at each temperature to generate sufficient data, and the error bars of the subsequent analysis data were determined.

Total structure factors, *S(q)*s, and pair correlation functions, $g(r)$s, of $Al_{77.8}Cu_{22.2}$ and $Al_{70}Cu_{20}Zr_{10}$ alloy liquids obtained from in situ HE-XRD at the temperatures of T_l+225 K, T_l+175 K, T_l+125 K, T_l+75 K, and T_l+25 K are shown in Figs. 1(a)-(d), respectively. *S(q)*s oscillate well around unity over the entire range of q, which indicates the high quality of the experimental data and appropriate data correction. The intensity of the first peak of *S(q)*s in two alloy liquids slightly grows with the decreasing temperature, showing an increase in the density [15]. The position of the first peak, q^1, and the nearest neighbor atomic distance, r^1, are listed in Table 1. The q^1 of two alloy liquids has no obvious change with temperature, but the value of q^1 in $Al_{70}Cu_{20}Zr_{10}$ is smaller than that in $Al_{77.8}Cu_{22.2}$ liquid alloy. The opposite situation is seen in r^1 due to the transformation from reciprocal space to real space. These differences indicate that the addition of Zr element has a significant influence on the structure of $Al_{77.8}Cu_{22.2}$ alloy liquid. Moreover, a pre-peak is also observed at about 1.0–2.0 $Å^{-1}$ for all temperatures in two alloy liquids, which is considered as a sign of medium-range order (MRO). The pre-peak in Al-Cu alloy liquid has been reported in previous studies [23-25], but the pre-peak in Al-Cu-Zr alloy liquids was never reported in the literature to the best of our knowledge. Moreover, the black open circles in Figs. 1(a) and (c) display the AIMD-simulated $S(q)$s, which shows a good agreement with the corresponding experimental data, indicating that thesesimulations are reliable.

Fig. 2 shows the temperature dependence of partial $g(r)$s of $Al_{77.8}Cu_{22.2}$ and

$Al_{70}Cu_{20}Zr_{10}$ liquid alloys. for both of them the intensity of all peaks is rather insensitive to the temperature, showing the structure is stable at high temperatures and no significant increase in ordering with cooling. The first peak of Al-Cu and Al-Zr partial $g(r)$s in all liquids has a high intensity and low first minimum, indicating Al and Cu atoms, and Al and Zr atoms have a very strong affinity and well-differentiated first

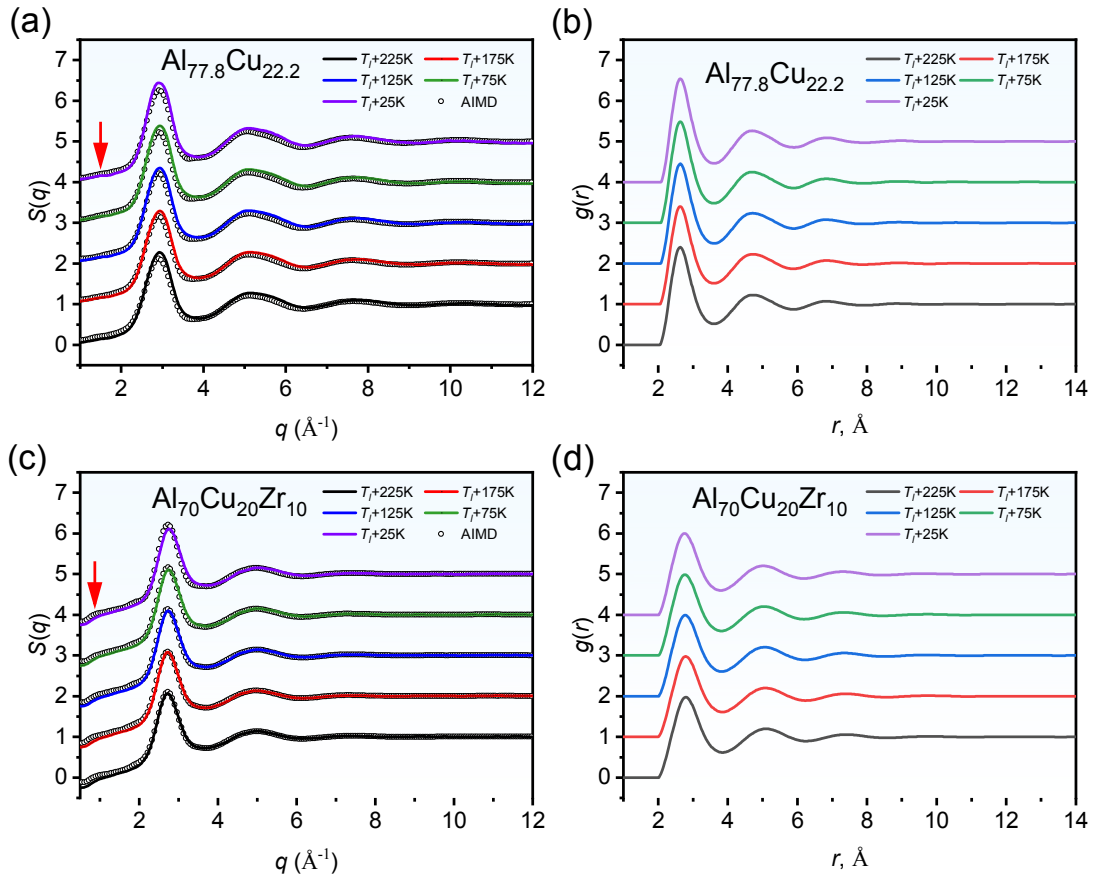

FIG. 1. Experimental structure factors, $S(q)$s, and pair-correlation functions, $g(r)$s (solid lines) of $Al_{77.8}Cu_{22.2}$ in (a) and (b), $Al_{70}Cu_{20}Zr_{10}$ in (c) and (d) at 225 K, 175 K, 125 K, 75 K, and 25 K above liquidus temperature, T_l, respectively shifted upwards by an amount 4, 3 2, 1 and 0 for the sake of clarity. The red arrows indicate the position of the pre-peaks, while the black open circles represent the AIMD simulation results.

Table 1 The position of the first peak in experimental *S(q)*s, q^1, and the nearest neighbor distance, r^1, of $Al_{77.8}Cu_{22.2}$ and $Al_{70}Cu_{20}Zr_{10}$ alloys liquids at each temperature

Temperature	$Al_{77.8}Cu_{22.2}$		$Al_{70}Cu_{20}Zr_{10}$	
	q^1 (Å^{-1})	r^1 (Å)	q^1 (Å^{-1})	r^1 (Å)
T_l+225 K	2.93	2.64	2.72	2.8
T_l+175 K	2.93	2.64	2.74	2.8
T_l+125 K	2.93	2.64	2.74	2.78
T_l+75 K	2.93	2.64	2.76	2.76
T_l+25 K	2.91	2.64	2.76	2.76

coordination layer. In comparison, the weak intensity of the first peak for Cu-Cu, Cu-Zr, and Zr-Zr partial *g*(*r*)s is found. Thus, it can be concluded that Cu and Zr atoms are mainly surrounded by Al atoms. It is also notable that the intensity of the second peak in Zr-Zr partial *g*(*r*) is higher than that of the first peak, indicating that these atoms tend to be arranged in the second shell layer. Such structural features suggest that the significant chemical short-range orders exist in the liquid, which leads to the Al and Zr atoms being alternately arranged in the liquid.

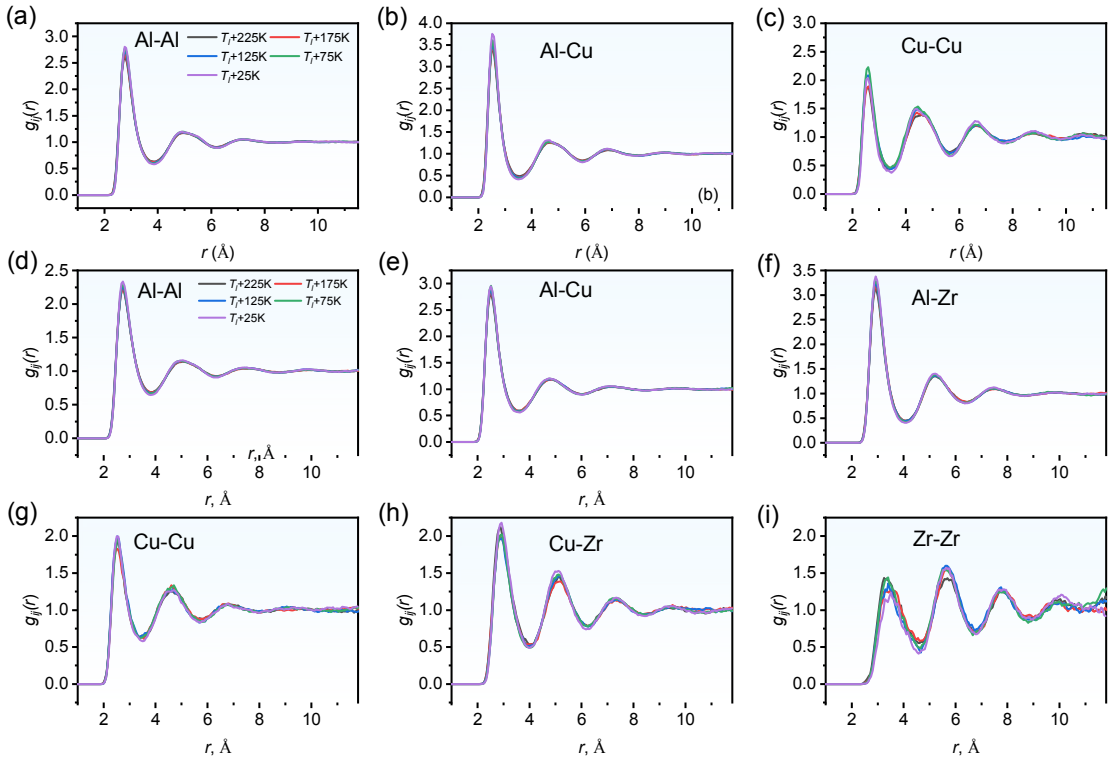

FIG. 2. Partial *g*(*r*)s of (a)-(c) $Al_{77.8}Cu_{22.2}$ and (d)-(i) $Al_{70}Cu_{20}Zr_{10}$ alloys liquids

obtained from the AIMD simulation at different temperatures.

The quality of the RMC fit of experimental *S(q)*s and AIMD-derived partial *g*(*r*)s at T_l+25 K for two liquid alloys is shown in supplementary Figs. S1-S2. The RMC simulations generally reproduce the experimental *S(q)*s and AIMD-derived partial *g*(*r*)s very well, ensuring strongly the reliability of the obtained atomic configurations. CNA [26-28] was used to analyze the SRO structures of the alloy liquids. In this method, each bond pair of atoms is classified by a set of three indices, jkl, which is computed from the

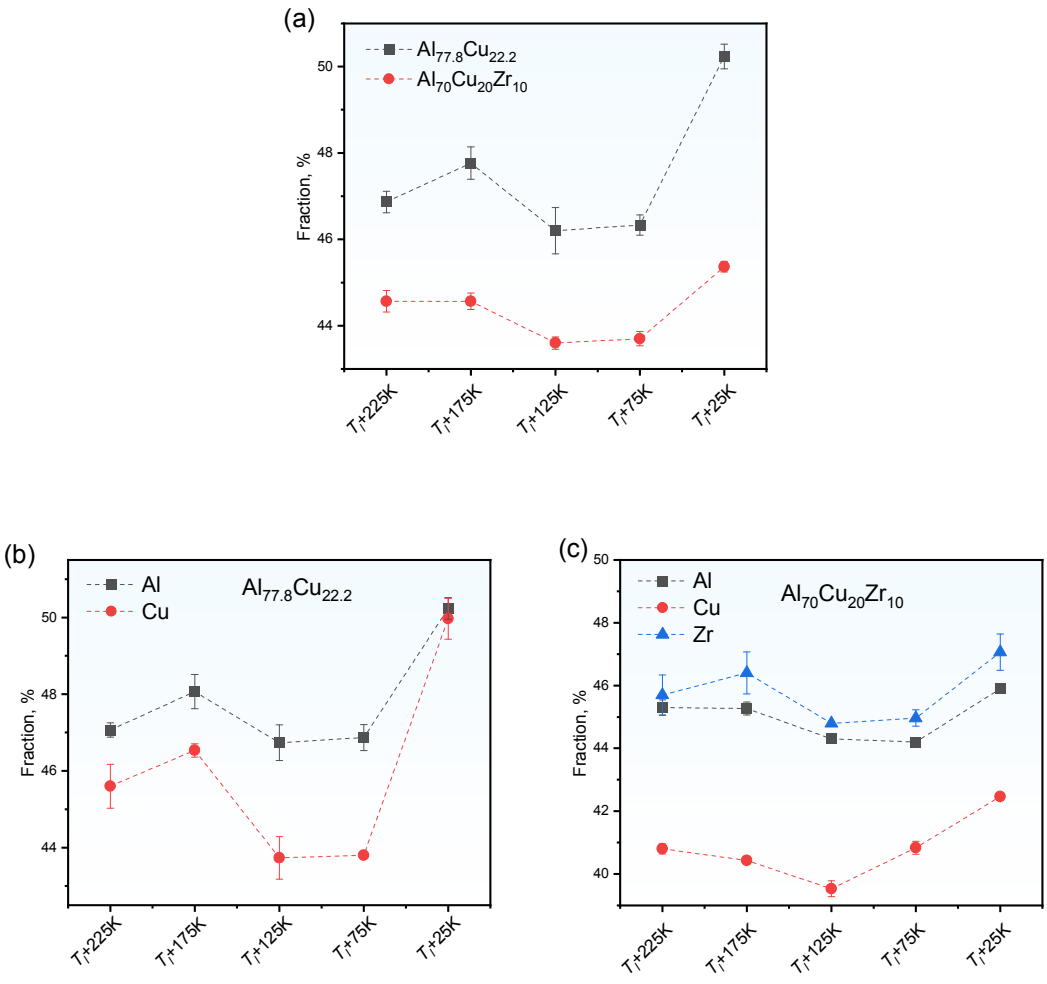

FIG. 3. Sum of fraction of index 555, 544 and 433 as a function of temperature for (a) total $Al_{77.8}Cu_{22.2}$ and $Al_{70}Cu_{20}Zr_{10}$ liquid alloys, (b) and (c) and for each component.

topology of the bonds that connect the surrounding neighbor atoms. The cutoff distance of each atom pair is chosen by the first minimum of partial $g(r)$s. Fig. 3(a) shows the sum of fraction of index 555, 544 and 433 that represent the ISROs of two alloy liquids at different temperatures. The content of ISROs is about 47.5% and 44% for $Al_{77.8}Cu_{22.2}$ and $Al_{70}Cu_{20}Zr_{10}$ alloy liquids, respectively. The ISROs of Al, Cu and Zr atoms in two alloy liquids was further analyzed and compared, as shown in Figs. 3(b)-3(c). The variation trend of the content of Al-centered ISROs with temperature is consistent with that of total ISROs, indicating that most of the ISROs in the liquid is Al-centered. The content of Al- and Cu-centered ISROs in $Al_{77.8}Cu_{22.2}$ alloy liquid is higher than that in $Al_{70}Cu_{20}Zr_{10}$ alloy liquid. The content of Zr-centered ISROs is higher than that of Al- and Cu-centered ISROs in $Al_{70}Cu_{20}Zr_{10}$ alloy liquid. These results show the content of ISROs decreases when adding Zr atoms in $Al_{77.8}Cu_{22.2}$ alloy liquid. The analysis of five-fold symmetry ordering also shows same result, see supplementary Fig. S3. ISROs usually is considered to be correlated with GFA due to the incompatibility with the transition symmetry of the crystal, and the more ISROs, the higher the GFA [29-32]. However, the above results show that the content of ISROs in $Al_{70}Cu_{20}Zr_{10}$ amorphous alloy liquid is lower than that in $Al_{77.8}Cu_{22.2}$ crystal-forming liquid. Therefore, it is difficult to explain the better GFA for $Al_{70}Cu_{20}Zr_{10}$ alloy liquid from this aspect.

Recently, Wang *et al.* [33] found that the variance of the cluster fractions in the high temperature liquids correlates well with the GFA instead of the cluster type and structure. Li *et al.* [34] also found that it may not be the characteristics of specific SRO, but the difference in the number of involved polyhedral types that reflects GFA. Here, we count the number of cluster type identified with Voronoi tessellation method and calculate the variance of the cluster fractions by an equation, $\delta^2=\sum_i \left(X_i-\mu\right)^2/N_c$, where X_i is the fraction of a particular type of cluster, μ is the average value of the fraction of all clusters and N_c is the number of the clusters in the calculation. As

shown in Fig. 4(a)-4(b), $Al_{70}Cu_{20}Zr_{10}$ amorphous alloy liquid has the lower variance value and the more cluster types than $Al_{77.8}Cu_{22.2}$ alloy liquid, which is consistent with previous conclusion that the lower the variance of the cluster fraction and the more cluster types, the better the GFA. This result indicates that the addition of Zr element increases the number of cluster types and make the distribution of cluster content more uniform, thus improves the GFA of $Al_{77.8}Cu_{22.2}$ alloy liquid.

MRO describes the structure information beyond the SRO and it is also considered as a powerful concept for understanding the glass formation. Here, we analyze the spatial correlation using a cluster correlation method [35]. All clusters are identified with Voronoi tessellation methods and are divided into 11 groups with the degree of the five-fold symmetry, f^5[36]. Figs. 4(c)-4(d) shows the correlation matrixes of C_{ij} at the lowest temperature investigated for $Al_{77.8}Cu_{22.2}$ and $Al_{70}Cu_{20}Zr_{10}$. The common feature in the two matrixes is that the value of C_{ij} at the bottom-right and up-left in the correlation matrix is larger than 0, while those at the up-right and bottom-left is smaller than 0. This implies that the clusters with $f^5>0.5$ or $f^5\leq0.3$ tend to connect with each other and the clusters with $f^5>0.5$ and $f^5\leq0.3$ tend to avoid each other. The C_{ij} value ranges from -1.0 to 1.7 in $Al_{77.8}Cu_{22.2}$, while the C_{ij} value ranges from -1.0 to 5.6 in $Al_{70}Cu_{20}Zr_{10}$, indicating the nonrandom spatial correlations of local structures are already present in the liquid and the stronger structure heterogeneity exists in $Al_{70}Cu_{20}Zr_{10}$. The local structural with the largest C_{ij} value in the two alloy liquids are $0.8<f^5\leq0.9$ and $0.9<f^5\leq1$, respectively. Such strong structure heterogeneity and spatial correlation in $Al_{70}Cu_{20}Zr_{10}$ will lead to the

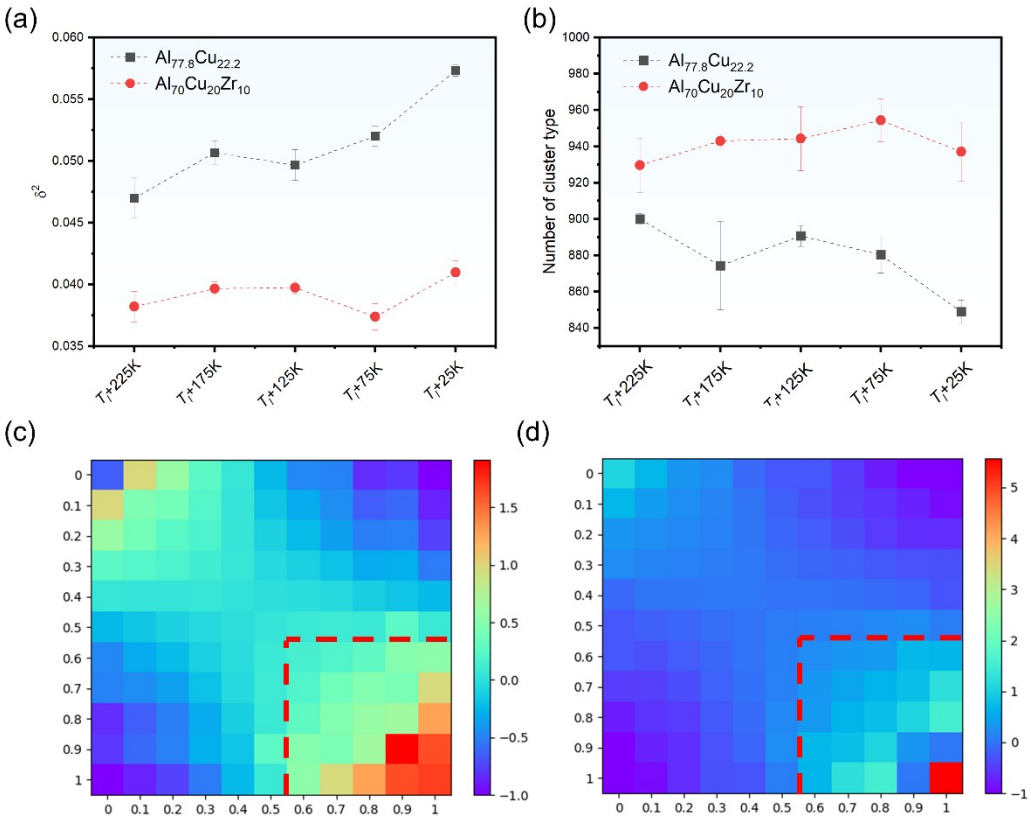

FIG. 4. (a) The variance of the cluster fractions, δ^2, and (b) the number of Voronoi polyhedral types of $Al_{77.8}Cu_{22.2}$ and $Al_{70}Cu_{20}Zr_{10}$ alloy liquids at different temperatures. Correlation matrixes of C_{ij} between clusters with different degree of the five-fold symmetry in (c) $Al_{77.8}Cu_{22.2}$ and (d) $Al_{70}Cu_{20}Zr_{10}$ alloy liquids at the lowest temperature investigated.

aggregation of clusters with $0.9<f^5\leq1$ and the formation of stable interpenetrating structures with high five-fold symmetry. A lot of studies [35-41] have shown that the enhanced connectivity of SRO clusters could be responsible for the better inheritance of structural heterogeneity, and the aggregation of ISRO clusters can cause the dynamic heterogeneity and slowdown, leading to the formation of glass.

Previous studies [42-44] have shown that the ISRO is not the dominant structure in Al-based metallic glasses and their GFA originates from the mixing of clusters of different sizes and types. Our this and previous studies [25] confirm these conclusions and gives a correlation between the MRO structure of the liquid and the GFA, *i.e.* the

structural heterogeneity of the liquid and correlation of clusters with high five-fold symmetry. We were surprised to find that the correlation is also present in a large number of metallic glass liquids dominated by ISROs [35,36], such as Cu-Zr, Mg-Zn-Y, suggesting the importance of MROs in the glass transition and this structural information might be a universal parameter related to the GFA. Some recent studies [45,46] have also pointed out that MROs can provide a stronger explanation for the glass formation than SROs, which supports our finding.

In summary, the structure of $Al_{77.8}Cu_{22.2}$ and $Al_{70}Cu_{20}Zr_{10}$ alloy liquids was investigated by combining HE-XRD, AIMD and RMC simulations. It was found that the GFA of Al-Cu-Zr alloy liquid is not related to the content of icosahedral short-range order, but to the diversity of cluster types and the uniformity of cluster content distribution on the SRO scale, and the structural heterogeneity and correlation of clusters with high five-fold symmetry on the MRO scale. These results reveal the atomic mechanism of Zr elements enhancing the GFA of the Al-Cu alloy liquid, and deepen the understanding of Al-based metallic glass formation.

Acknowledgements

This work was supported by the National Key R&D Program of China (2017YFA0403802), the National Natural Science Foundation of China (91860121, 51727802), and the National Science and Technology Major Project of China (2017-Ⅶ-0008-0102). Support of the synchrotron high-energy X-ray diffraction of BL13W1 of the Shanghai Synchrotron Radiation Facility (SSRF), China, is gratefully acknowledged. We also acknowledge the CINES and IDRIS under Project No. INP2227/72914, and CIMENT/GRICAD for the computational resources. This work was performed within the framework of the Centre of Excellence of Multifunctional Architectured Materials "CEMAM" ANR-10-LABX-44-01 funded by the "Investments for the Future" Program. This work has been partially supported by MIAI@Grenoble Alpes (ANR-19-P3IA-0003). Fruitful discussion within the French collaborative network in in artificial intelligence in materials science GDR CNRS 2123 (IAMAT) is also acknowledged. This work was also funded by China

Scholarship Council. The authors also wish to thank Dr. P Jarry for helpful discussions.

References

[1] W. Klement, R.H. Willens, P.O.L. Duwez, Nature 187 (1960) 869-870.

[2] P. Chaudhari, D. Turnbull, Science 199 (1978) 11-21.

[3] D.B. Miracle, Nat. Mater. 3 (2004) 697-702.

[4] H.W. Sheng, W.K. Luo, F.M. Alamgir, J.M. Bai, E. Ma, Nature 439 (2006) 419-425.

[5] A. Inoue, T. Zhang, T. Masumoto, J. Non-Cryst. Solids 156 (1993) 473-480.

[6] A. Inoue, Acta Mater. 48 (2000) 279-306.

[7] A. Inoue. Prog. Mater. Sci. 43 (1998) 365-520.

[8] Y. Wu, H. Wang, H.H. Wu, Z.Y. Zhang, X.D. Hui, G.L. Chen, D. Ma, X.L. Wang, Z.P. Lu, Acta Mater. 59 (2011) 2928-2936.

[9] J. Mu, H. Fu, Z. Zhu, A. Wang, H. Li, Z. Hu, H. Zhang, Adv. Eng. Mater. 11 (2009) 530-532.

[10] T. Shindo, Y. Waseda, A. Inoue, Mater. Trans. 44 (2003) 351-357.

[11] H.Z. Fang, X. Hui, G.L. Chen, Z.K. Liu, Appl. Phys. Lett. 94 (2009) 091904.

[12] Y.Q. Cheng, E. Ma, H.W. Sheng, Phys. Rev. Lett. 102 (2009) 245501.

[13] L.C.R. Aliaga, L.V.P.C. Lima, G.M.B. Domingues, I.N. Bastos, G.A. Evangelakis, Mater. Res. Express 6 (2019) 045202.

[14] T.K. Gu, J.Y. Qin, X.F. Bian, Appl. Phys. Lett. 91 (2007) 081907.

[15] N.A. Mauro, V. Wessels, J.C. Bendert, S. Klein, A.K. Gangopadhyay, M.J. Kramer, S.G. Hao, G.E. Rustan, A. Kreyssig, A.I. Goldman, K.F. Kelton, Phys. Rev. B 83 (2011) 184109.

[16] M.L. Johnson, M.E. Blodgett, K.A. Lokshin, N.A. Mauro, J. Neuefeind, C. Pueblo, D.G. Quirinale, A.J. Vogt, T. Egami, A.I. Goldman, K.F. Kelton, Phys. Rev. B 93 (2016) 054203.

[17] A.P. Hammersley, J. Appl. Crystallogr. 49 (2016) 646-652.

[18] X. Qiu, J.W. Thompson, S.J.L. Billinge, J. Appl. Crystallogr. 37 (2004) 678-678.

[19] G. Kresse, J. Furthmüller, Comput. Mater. Sci. 6 (1996) 15-50.

[20] D.M. Ceperley, B.J. Alder, Phys. Rev. Lett. 45 (1980) 566.

[21] S. Le Roux, V. Petkov, J. Appl. Cryst. 43 (2010) 181-185.

[22] O. Gereben, P. Jovari, L. Temleitner, L. Pusztai, J Optoelectron Adv M 9 (2007) 3021.

[23] J. Brillo, A. Bytchkov, I. Egry, L. Hennet, G. Mathiak, I. Pozdnyakova, D.L. Price, D. Thiaudiere, D. Zanghi, J. Non-Cryst. Solids 352 (2006) 4008-4012.

[24] N. Jakse, A. Pasturel, Phys. Rev. B 94 (2016) 224201.

[25] S. Cao S, L. Zeng, M. Xia, P Yu, W. Lu, J. Li, J. Mol. Liq. 357 (2022) 119143.

[26] A. Stukowski, Modell. Simul. Mater. Sci. Eng. 18 (2009) 015012.

[27] A. Stukowski, Modell. Simul. Mater. Sci. Eng. 20 (2012) 045021.

[28] A.S. Clarke, H. Jónsson, Phys. Rev. E 47 (1993) 3975.

[29] H. Tanaka, J. Phys. Condens. Matter 15 (2003) L491.

[30] N. Jakse N, A. Pasturel, Appl. Phys. Lett. 93 (2008) 113104.

[31] N. Jakse, A. Pasturel, Phys. Rev. B 78 (2008) 214204.

[32] H. Chen, D. Li, Y. Zhao, B. Qu, R. Zhou, B. Zhang, Phys. Chem. Chem. Phys. 21 (2019) 4209-4214.

[33] J. Wang, A. Agrawal, K. Flores, Acta Mater. 171 (2019) 163-169.

[34] M.X. Li, Y.T. Sun, C. Wang, L.W. Hu, S. Sohn, J. Schroers, W.H. Wang, Y.H. Liu, Nat. Mater. 21 (2022) 165-172.

[35] M. Li, C.Z. Wang, S.G. Hao, M.J. Kramer, K.M. Ho, Phys. Rev. B 80 (2009) 184201.

[36] Y.C. Hu, F.X. Li, M.Z. Li, H.Y. Bai, W.H. Wang, Nat. Commun. 6, 8310 (2015).

[37] X.J. Liu, S.D. Wang, H.Y. Fan, Y.F. Ye, H. Wang, Y. Wu, Z.P. Lu, Intermetallics 101 (2018) 133-143.

[38] A. Pasturel, N. Jakse, J. Chem. Phys. 146 (2017) 184502.

[39] A. Pasturel, N. Jakse, npj Comput. Mater. 3 (2017) 33.

[40] H.L. Peng, M.Z. Li, H.W. Wang, C.Z. Wang, K.M. Ho, Appl. Phys. Lett. 96 (2010) 021901.

[41] W. Lu, J.C. Tseng, A. Feng, J. Shen, J. Non-Cryst. Solids 564 (2021) 120834.

[42] H.W. Sheng, Y.Q. Cheng, P.L. Lee, S.D. Shastri, E. Ma, Acta Mater. 56 (2008) 6264-6272.

[43] Y.Q. Cheng, E. Ma, Prog. Mater. Sci. 56 (2011) 379-473.

[44] F.R. Wang, H.P. Zhang, M.Z. Li, J. Alloys Compd. 763 (2018) 392-398.

[45] X. Fan, Y. Sun, C.Z. Wang, K.M. Ho, M.S. Altman, L. Huang, Phys. Rev. B 101 (2020) 214104.

[46] C.W. Ryu, T. Egami, Phys. Rev. E 104 (2021) 064109.